University of Victoria

Development and Validation of a Direct Ink Writing Platform for Lignin-Based Materials

Honours Thesis

Oscar O'Regan

Department of Mechanical Engineering

Supervisor: Prof. Samira Gharehkhani

April 2026

Abstract

Lignin is the second most abundant renewable polymer on earth, trailing only cellulose, yet much of it is still burned as a low-value fuel. In parallel, direct ink writing (DIW) has become an increasingly important additive manufacturing method because it supports a broad range of applications and can be used with many materials. However, most printable materials still remain conventional polymer-based feedstocks, so this work investigates lignin's potential as a more sustainable material for DIW printing.

An open-source Printess bioprinter was assembled, modified, and validated to provide a reliable platform for syringe-based extrusion. A review of lignin-based DIW inks identified a lignin–Pluronic F127 system as a promising starting point because of its high lignin content, simple chemistry, and printability under room-temperature conditions. Experimental work then focused on developing and refining this ink through variations in pH, particle size, drying method, and preparation route. The resulting formulations were assessed through printability tests, material behaviour in different environments, and preliminary strength observations. Throughout testing, printer improvements were also made to increase consistency and reliability.

This work provides a foundation for using lignin as a DIW material and supports the broader development of more sustainable feedstocks for extrusion-based additive manufacturing.

Contents

List of Figures

List of Tables

1 Introduction

1.1 Background

Lignin is the second most abundant renewable polymer on Earth and a major structural component of wood. It contributes rigidity and compressive strength in plant cell walls, but much of the lignin produced through pulping and paper processing is still burned rather than converted into higher-value products [5, 6]. That makes lignin a useful candidate for sustainable materials development, especially in processes that can handle high solid loading and paste-like feedstocks.

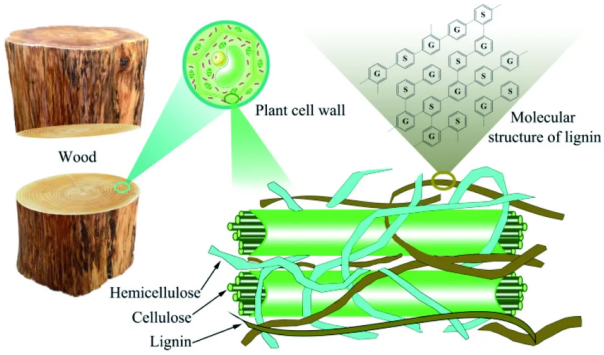

(a) Lignin as a structural component of wood, adapted from Li et al. [7].

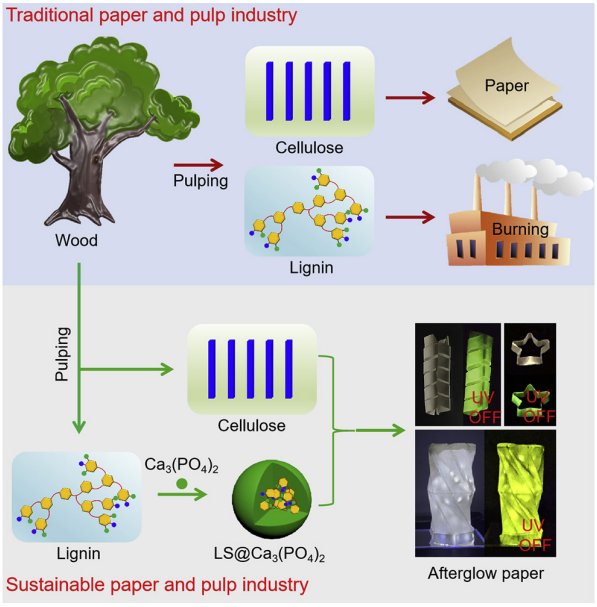

(b) Lignin as an underused pulping byproduct, adapted from Yang et al. [8].

Figure 1: Background context for why lignin is an attractive feedstock for sustainable materials development.

Additive manufacturing offers a way to produce customized parts with minimal tooling, but many common printing routes still depend on thermoplastics or photocurable resins. Direct ink writing (DIW) is different because it extrudes a prepared ink through a nozzle rather than melting a filament or curing a liquid resin. DIW is already used for applications such as bioprinting, tissue scaffolds, soft materials, printed electronics, and energy-related devices because it can process viscous functional inks under relatively mild conditions [4, 6]. That makes it a strong fit for lignin-rich formulations, which are more naturally handled as pastes or gels than as filaments or resins [1, 4].

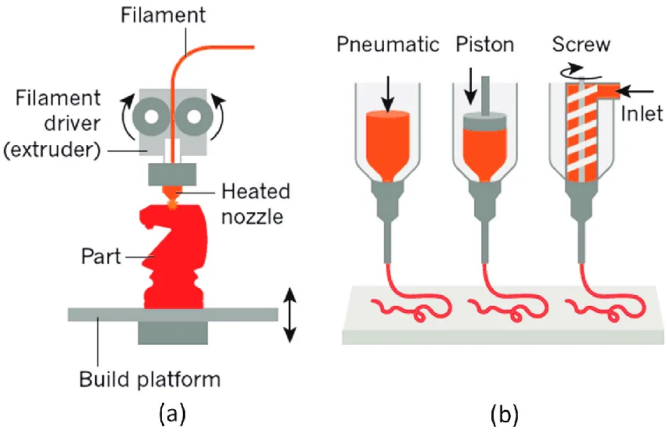

(a) Comparison of FDM and DIW deposition concepts, adapted from Liu and Yan [9].

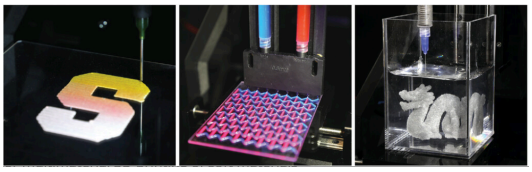

(b) Representative DIW print examples, adapted from Weiss et al. [4].

Figure 2: Direct ink writing is better suited to viscous inks than filament- or resin-based routes.

1.2 Objectives

My main objectives were:

1. assemble and validate a low-cost DIW printer based on the Printess architecture;
2. establish a repeatable CAD-to-print workflow for syringe-based extrusion;
3. review lignin-based DIW ink systems and select a practical starting formulation;
4. develop and refine a workable lignin-rich ink through screening of lignin source, preparation route, and pH; and
5. demonstrate preliminary printing, post-processing, and basic performance evaluation of lignin-based structures.

2 Literature Review

2.1 Direct Ink Writing and Lignin

Direct ink writing is an extrusion-based additive manufacturing process in which a formulated ink is deposited through a nozzle along a programmed path [4, 6]. A key advantage of DIW is that it can process materials that are too viscous for inkjet-style deposition and do not need to be converted into a filament or photocurable resin. This is why DIW is widely used for soft materials, bioinks, ceramic pastes, conductive inks, and other functional formulations that need gentle processing conditions [4, 6].

For DIW to work well, the material has to satisfy two competing requirements. It must flow when pressure is applied in the syringe or nozzle, but it must also recover enough structure

after extrusion to hold its shape. In practice, that usually means the ink needs strong shear-thinning behaviour and sufficient yield stress or elasticity after deposition. This balance between flow and shape retention is one of the central challenges in lignin-based printing [1, 10].

Lignin is attractive in this context because it is abundant, relatively inexpensive, and can contribute stiffness, UV resistance, and thermal stability [1, 5]. At the same time, lignin-rich mixtures can be difficult to extrude consistently, so DIW offers a practical route to test these materials directly as pastes rather than forcing them into a filament- or resin-based process [6, 2].

2.2 Candidate Ink Systems

Three candidate systems were the most relevant to this project. The first used lignosulfonate, methyl cellulose, and glycerol in a simple water-based formulation [2]. The second used lignin and Pluronic F127 to produce self-supporting direct-ink-printed lignin scaffolds [1]. The third used organosolv lignin and hydroxypropyl cellulose to produce fully bio-based aqueous inks with promising mechanical properties [3]. These are summarized in Table 1.

Table 1: Candidate lignin-based DIW ink systems considered in this work.

System	Key strengths	Main limitation for this project
Lignosulfonate / methyl cellulose / glycerol [2]	Simple water-based chemistry, high lignin loading, recyclable by rehydration	Uses lignosulfonate rather than the alkali lignin available for this work
Lignin / Pluronic F127 [1]	High lignin loading, self-supporting builds, simple room-temperature preparation	Requires careful control of lignin condition and post-processing
Organosolv lignin / hydroxypropyl cellulose [3]	Good alignment and promising stiffness	More specialized materials system than was practical for this project

The lignin–F127 system reported by Jiang *et al.* was the most influential paper for me because it directly demonstrated that lignin-rich DIW inks can form self-supporting structures with useful mechanical performance [1]. Figure 3 shows example printed features and selected reported properties from that study.

(a) Example lignin–F127 print.

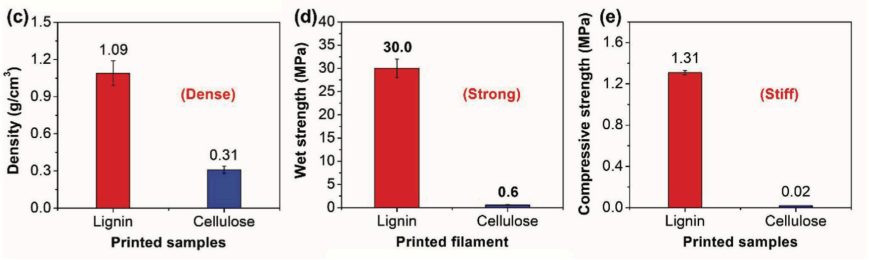

(b) Selected density and strength data.

Figure 3: Representative performance of the selected lignin–F127 ink system, adapted from Jiang et al. [1].

The lignosulfonate-based system was appealing because of its simplicity and recyclability. It is a water-only formulation, it can be mixed at room temperature, and it can be ground and rehydrated for reprinting [2]. The tradeoff is that it tends to show more shrinkage and lower strength, and the methyl cellulose to glycerol balance has to be tuned carefully to manage wet shape retention, cracking, and stiffness. That made it attractive as a baseline but less suitable as the main route for this project.

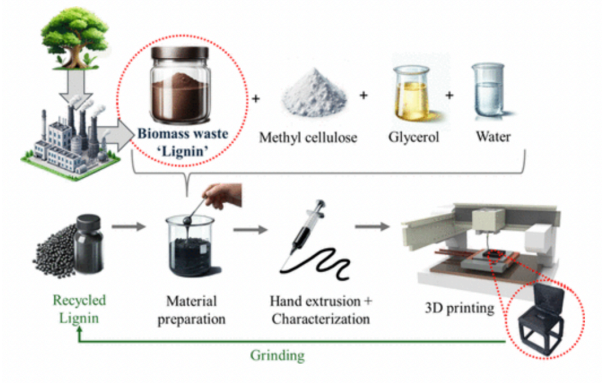

(a) Water-based LS/MC/G process route.

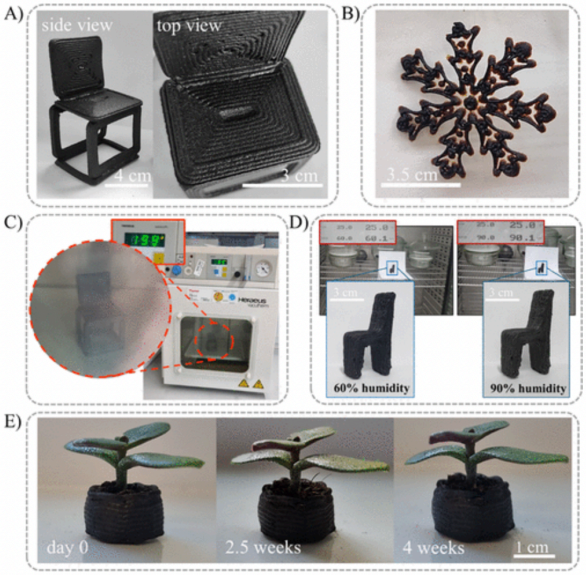

(b) Representative printed examples and aging behaviour.

Figure 4: Figures that helped frame the lignosulfonate / methyl cellulose / glycerol route as a simple and recyclable baseline system, adapted from Balk et al. [2].

The organosolv lignin / hydroxypropyl cellulose route was also promising because extrusion-induced alignment can increase stiffness and introduce anisotropy [3]. At the same time, it depends on mixed solvents, has a narrower formulation window, and requires curing, which

would have added more complexity to a project that already included building the printer itself.

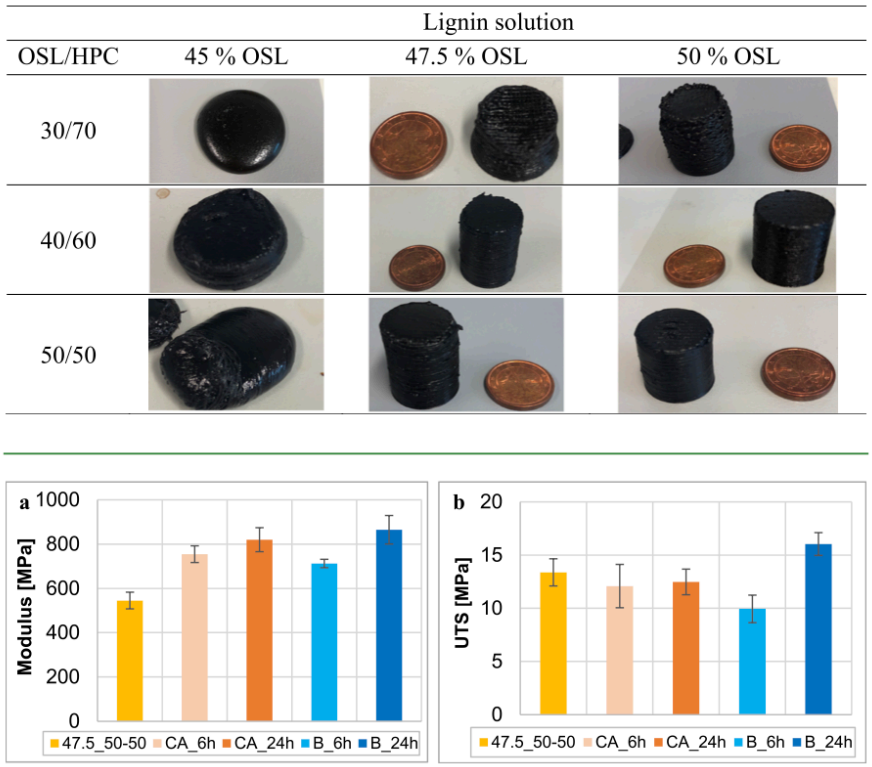

Figure 5: OSL/HPC formulation window and mechanical summary, adapted from Ebers and Laborie [3].

2.3 Selection of the Lignin–F127 Route

I selected the lignin–F127 route because it offered the best balance of lignin loading, simplicity, and demonstrated printability [1]. Pluronic F127 was also attractive because its gel-forming behaviour in water is well established, and it was easy to source at reasonable cost [11].

2.4 Choice of Lignin Source Within the Selected Ink Route

After selecting the lignin–F127 route, I then chose a lignin source that was practical to obtain and work with. The literature shows that this type of ink system can be used with different technical lignins, including kraft-type lignins [5, 6]. For this project, I used alkali lignin because it was accessible, relatively inexpensive, and realistic to source for experimental formulation work [12, 13, 5].

Alkali lignin is lignin recovered from alkaline pulping or alkaline extraction processes. Kraft lignin belongs to this same general family, since it is produced from the kraft pulping process,

and in practice it is often recovered from black liquor by acid precipitation and washing during downstream recovery or purification [5, 6]. For this work, alkali lignin gave a good balance between cost, availability, and relevance [12, 13]. In Canada especially, lignin from forestry and pulping streams is a practical feedstock to think about [5, 6].

3 Experimental Platform

3.1 Printess Platform

I based the printer on the open-source Printess platform reported by Weiss *et al.* [4, 14]. I chose it because it provides a compact syringe-based DIW architecture at much lower cost than many commercial bioprinters while still remaining customizable. Figure 6 shows the published platform concept that guided the build.

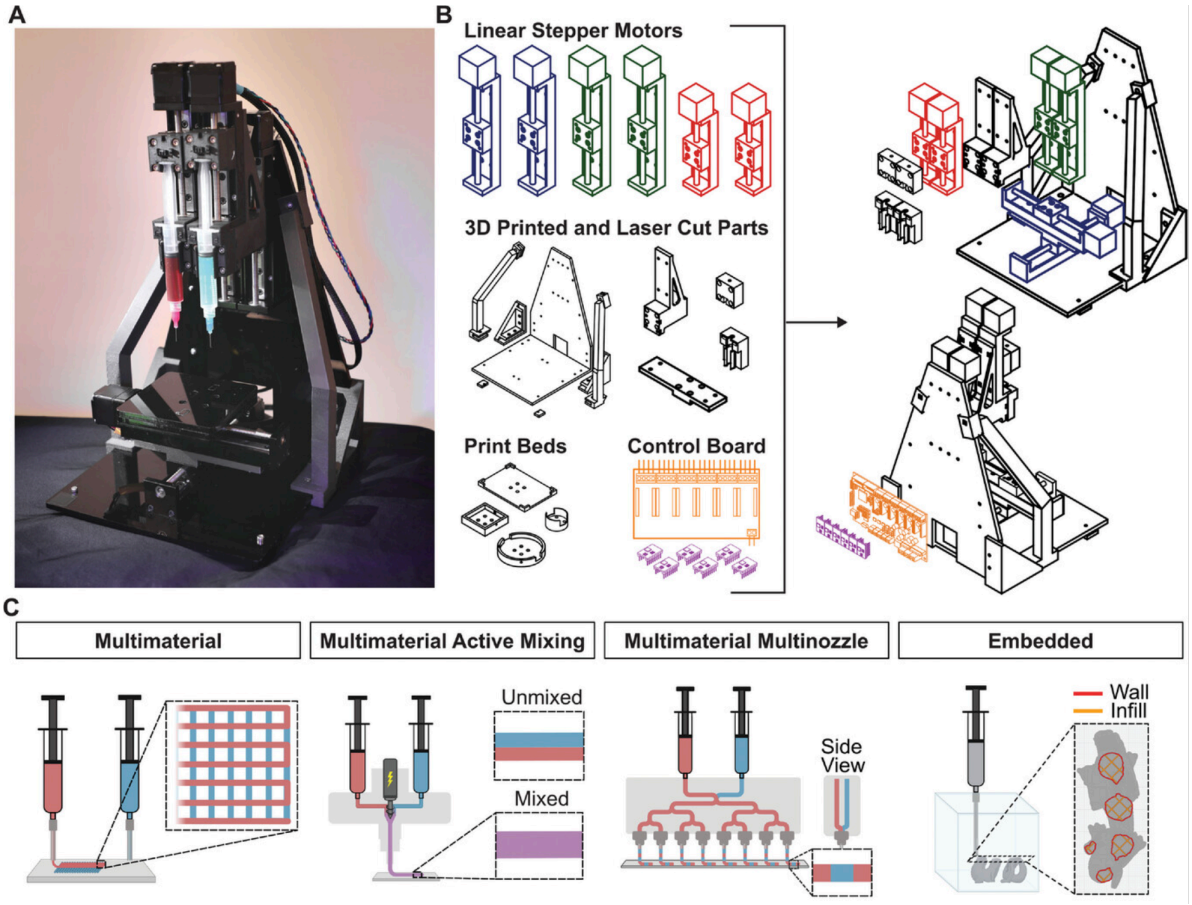

Figure 6: Printess platform overview and modular architecture, adapted from Weiss et al. [4].

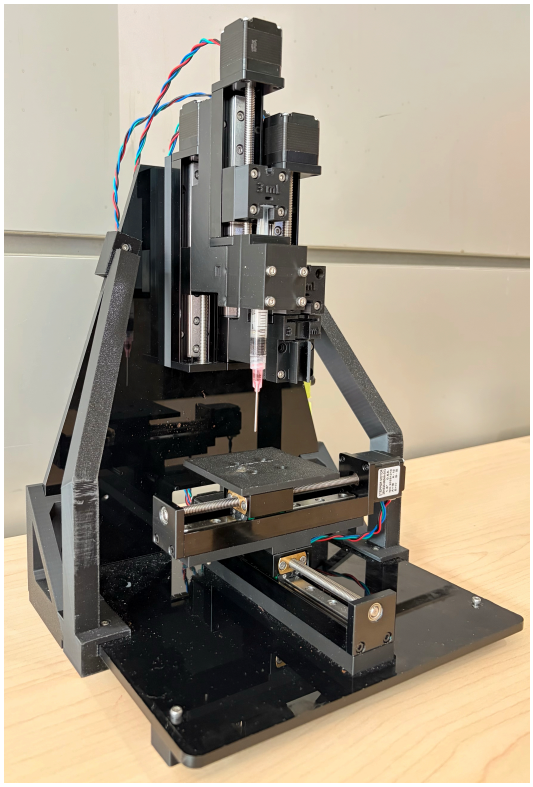

Figure 7: Completed syringe-based DIW printer assembled for this project.

3.2 Parts Procurement and Cost

All mechanical and electrical components required for the printer were sourced from a combination of McMaster-Carr, Amazon, and AliExpress. Initial component scouting was conducted to evaluate availability and pricing. After comparison, it was determined that ordering primarily through AliExpress resulted in significant cost savings while maintaining acceptable component quality.

The total cost of the printer build was approximately CAD $584.64.

Table 2: Itemized bill of materials for the printer build.

Component / item	Supplier	Cost (CAD)
Heat-set threaded inserts (50 pcs)	AliExpress	6.05
JST XH2.54 connector pins (200 pcs)	AliExpress	6.13
DIN562 stainless thin nuts (50 pcs)	AliExpress	3.69
NEMA 11 linear module, 50 mm stroke (2 pcs)	AliExpress	71.71
NEMA 11 linear module, 100 mm stroke (4 pcs)	AliExpress	143.43
M3 stainless socket head screws, 45 mm (50 pcs)	AliExpress	6.44
M3 stainless socket head screws, 12 mm (50 pcs)	AliExpress	3.66
BIGTREETECH Octopus Pro V1.0 + TMC2209 drivers	AliExpress	102.68
Stainless steel dispensing needles (18G and 20G packs)	McMaster-Carr	66.00
BD 3 mL Luer-lock syringes (200 pcs)	Amazon Canada	56.50
24 V, 2 A DC power supply adapter	Amazon Canada	19.03
Black acrylic sheet panels, 12 in × 12 in × 6 mm (2 pcs)	Amazon Canada	49.16
Dupont jumper wire kit (120 pcs)	Amazon Canada	11.19
Shipping, customs, and import fees	UPS Customs	38.97
Total project cost		584.64

3.3 Mechanical Assembly

All structural components were fabricated using PLA filament at the UVic Makerspace. The design files were obtained directly from the Printess GitHub repository [14].

The mechanical assembly process proceeded largely without major complications. However, discrepancies between the documented NEMA 11 specifications and the dimensions of the received components required modification of the original design. The linear stepper motors supplied had updated mounting dimensions relative to those shown in the online documentation. As a result, the mounting holes in the laser-cut frame components did not align with the motor housing.

To resolve this issue, adapter plates were designed in CAD and fabricated via 3D printing to correct the mounting hole spacing and enable secure attachment of the motors to the frame. In addition, the Printess Z-axis and X–Y axis STEP files were modified to ensure proper alignment between the motor mounting holes and the selected stepper motors.

The use of adapter plates required more fasteners than originally anticipated and prevented

the use of all four mounting holes for each motor. In some cases, only two mounting holes could be utilized. Testing confirmed that this configuration still provided sufficient structural stability, but it remains a minor structural limitation that could be improved in future design iterations.

An adjustment was made to the syringe barrel holder after initial fabrication. The component was originally printed in an orientation that resulted in weaker inter-layer bonding along the primary load direction. It was subsequently reprinted with the layer lines oriented perpendicular to the expected stress direction, which significantly improved structural rigidity and durability.

Following these modifications, the mechanical assembly was completed successfully, and all motion axes operated smoothly under manual testing.

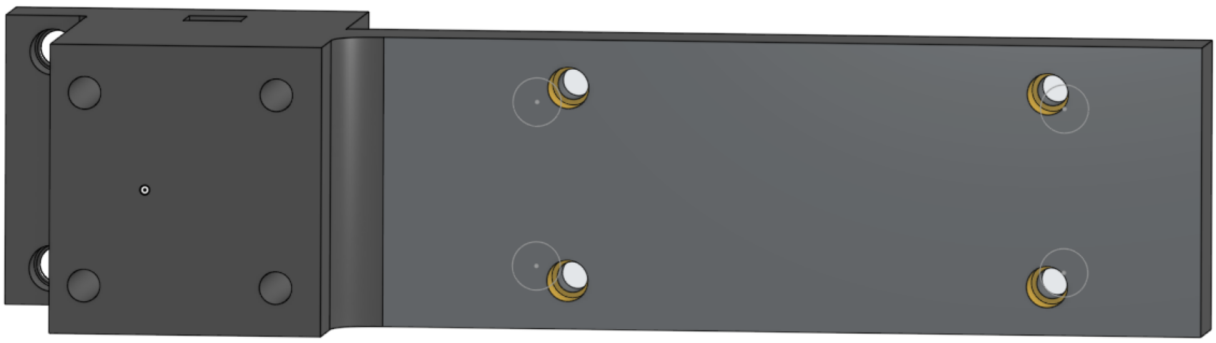

(a) Modified Z-axis holder.

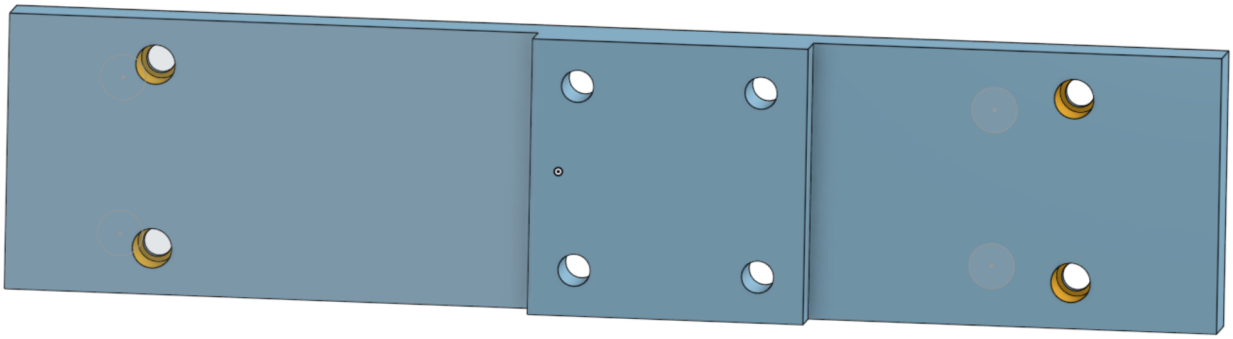

(b) Modified XY-axis connector.

Figure 8: Modified CAD models, light grey sketches indicate original mount hole positions.

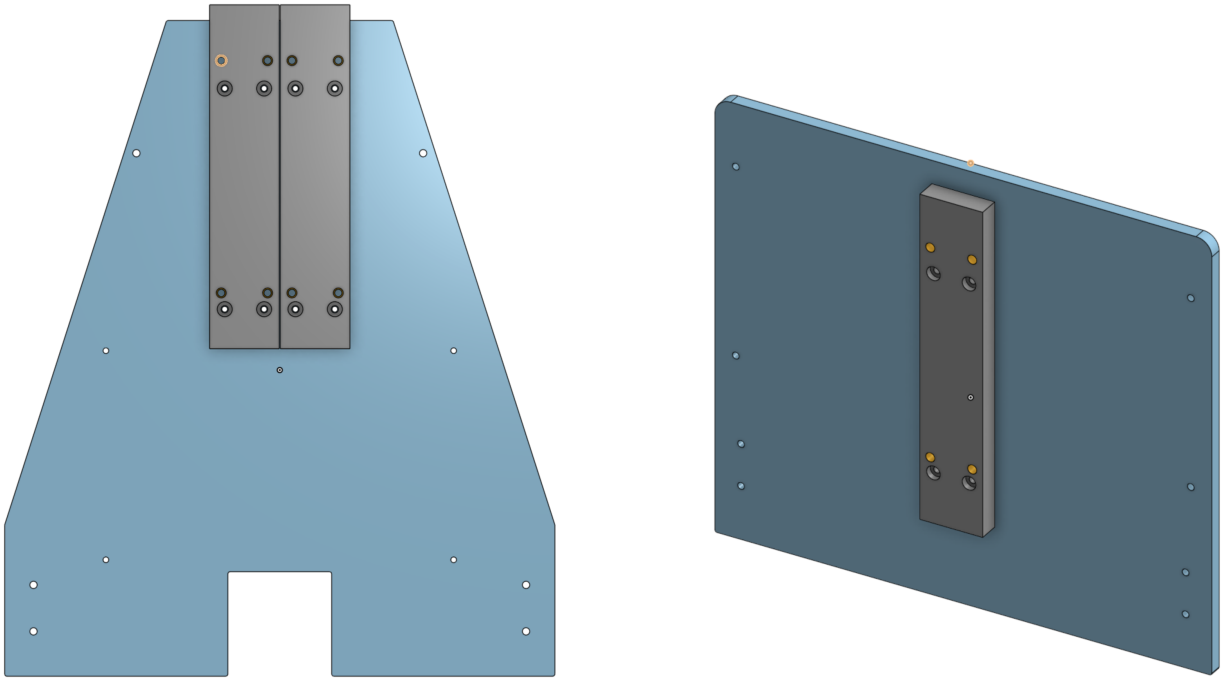

(a) Installed adapters on back plate assembly.

(b) Installed adapter on base plate assembly.

Figure 9: Custom 3D printed motor adapter plates designed to correct mounting hole spacing and enable proper motor alignment within the Printess frame.

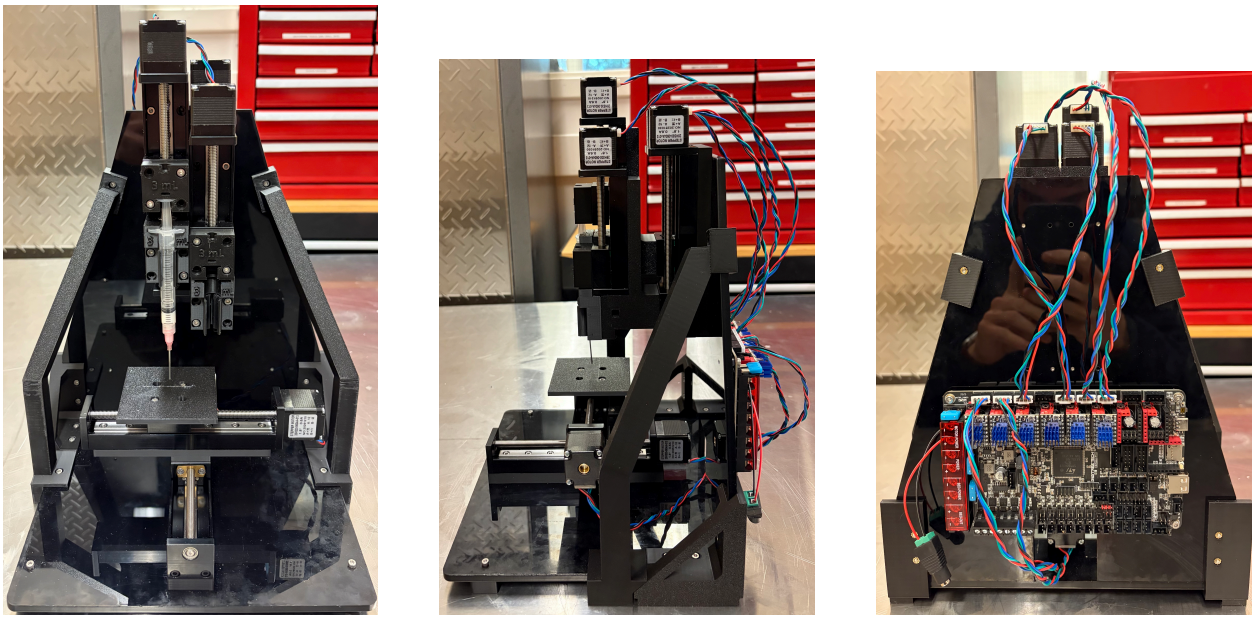

(a) Printer Front.

(b) Printer Side.

(c) Printer Back.

Figure 10: Printer.

3.4 Electrical Integration and Firmware Configuration

The printer was configured using Marlin firmware [15], modified and compiled within Visual Studio Code. Pronterface was used for direct motor control and motion verification.

Initial challenges included ensuring correct firmware installation, driver configuration, and motor mapping. During preliminary testing, certain motors were wired to incorrect axes, resulting in the motors not responding to commands.

One of the most time-intensive tasks during this phase was the crimping of JST connectors for stepper motor wiring. Proper crimping was essential to ensure reliable electrical contact. Inadequately crimped connectors resulted in intermittent electrical connections or wire detachment. Precision crimping techniques were used to improve long-term electrical reliability.

Upon completion of the wiring and firmware configuration, all axes were successfully controlled through Pronterface, confirming proper hardware–software integration.

3.5 CAD-to-G-Code Workflow Development

After establishing reliable axis motion, the next objective was to develop a consistent workflow for converting CAD models into executable G-code compatible with the Printess extrusion system. The process involved exporting CAD geometries as STL files, configuring a custom printer profile in Ultimaker Cura [16] to match the Printess build volume and motion parameters, and slicing the models accordingly. Print settings within Cura were adjusted to improve material deposition and dimensional accuracy with the syringe-based extrusion system. The generated G-code was then further modified to meet the specific control requirements of the extrusion system.

The default G-code generated by Cura required substantial modification. All extruder heating and temperature control commands were removed because the DIW system does not use thermoplastic extrusion. Standard filament-based extrusion commands were replaced with syringe flow control instructions. A custom Python script provided in the Printess documentation was then used to convert the modified G-code into the required format.

During this process, a recurring issue was encountered in which the Python script did not correctly convert extrusion commands unless a solitary “B” command was manually inserted at the beginning of the file. After identifying this requirement, a repeatable and reliable G-code conversion workflow was established.

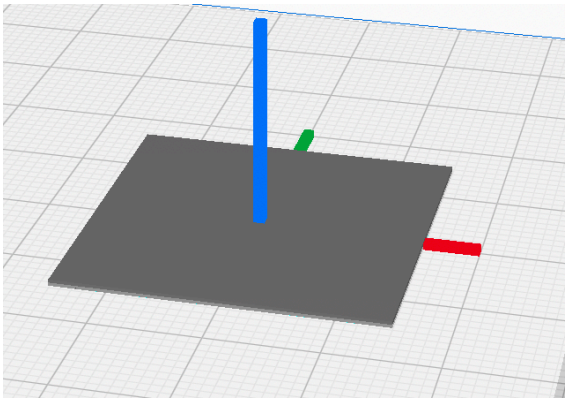

(a) STL file.

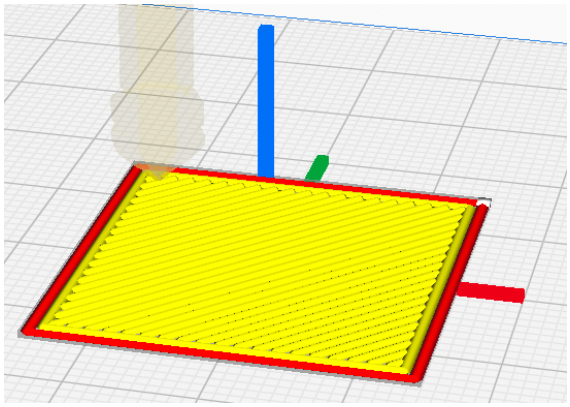

(b) Sliced file.

```
;FLAVOR:Marlin
;TIME:218
;Filament used: 0.0852018m, 0m
;Layer height: 0.6
;MINX:-14.5
;MINY:-14.5
;MINZ:0.6
;MAXX:14.5
;MAXY:14.5
;MAXZ:0.6
;TARGET_MACHINE.NAME:Unknown
;Generated with
Cura_SteamEngine 5.11.0
M104 S245
M105
M109 S245
G90
Z_syringe_diameter = 8.6
A_syringe_diameter = 8.6
Z_nozzle_diameter = 0.9521
A_nozzle_diameter = 0.9521
extrusion_coefficient = 1

G1 B0.1 F400
M82 ;absolute extrusion mode
G92 E0
G92 E0
G1 F120 E-6.5
;LAYER_COUNT:1
;LAYER:0
M107
;MESH:BP-Test (1).stl
G0 F300 X14.5 Y14.5 Z0.6
;TYPE:WALL-OUTER
G1 F120 E0
G1 F300 X-14.5 Y14.5 E2.72753
G1 X-14.5 Y-14.5 E5.45506
G1 X14.5 Y-14.5 E8.18259
G1 X14.5 Y14.5 E10.91012
G0 X14.017 Y14.5
G0 X13.938 Y13.938
G0 X12.942 Y12.972
G0 X13.548 Y13.548
```

```
G90
Z_syringe_diameter = 8.6
A_syringe_diameter = 8.6
Z_nozzle_diameter = 0.9521
A_nozzle_diameter = 0.9521
extrusion_coefficient = 1
G21
B (solitary "B")


G0 F300 X14.5 Y14.5 Z0.6
G1 Z0.6 F200.0

G91
G1 B0.1 F400
G92 B0

G90

;TYPE:WALL-OUTER
G1 F300 X-14.5 Y14.5
E2.72753
G1 X-14.5 Y-14.5 E5.45506
G1 X14.5 Y-14.5 E8.18259
G1 X14.5 Y14.5 E10.91012
G0 X14.017 Y14.5
G0 X13.938 Y13.938
G0 X12.942 Y12.972
G0 X13.548 Y13.548
```

```
G90
G21


G0 X14.5 Y14.5 Z0.6
F300.0
G1 Z1 B0.0 F200.0

G91
G1 B0.1 F400
G92 B0

G90

;TYPE:WALL-OUTER
G1 X-14.5 Y14.5
B0.251 F300.0
G1 X-14.5 Y-14.5
B0.607
G1 X14.5 Y-14.5
B0.962
G1 X14.5 Y14.5 B1.318
G0 X14.017 Y14.5
G0 X13.938 Y13.938
G0 X12.942 Y12.972
G0 X13.548 Y13.548
```

(c) Respectively: default G-code, edited G-code, modified G-code (Python script).

Figure 11: CAD-to-G-code workflow.

This workflow enabled consistent translation from digital geometry to physical extrusion commands.

3.6 Calibration and Validation

Following successful G-code execution, the printer underwent calibration procedures to improve deposition accuracy. The axes were manually homed, and the global coordinate system was initialized. Particular attention was given to the Z-offset calibration to ensure appropriate nozzle-to-bed clearance. The Z-offset was adjusted incrementally until slight contact between the nozzle and the build surface was observed. This ensured adequate adhesion during initial layer deposition while preventing excessive compression of the extruded material. After calibration, the printer demonstrated consistent positional accuracy and stable motion across all axes.

3.7 Initial Extrusion Testing with Surrogate Material

Before introducing lignin-based extrusion materials, the printer was validated using toothpaste as a surrogate test material. Toothpaste was selected due to its rheological properties, including high viscosity at rest and shear-thinning behavior under applied stress. These properties make it representative of many DIW-compatible materials.

Extrusion tests were conducted to optimize flow rate, travel speed, and line width. The material exhibited stable extrusion behavior, with minimal leakage and satisfactory geometric fidelity. Line uniformity remained consistent under calibrated conditions, while additional testing would still be needed to assess layer stacking performance.

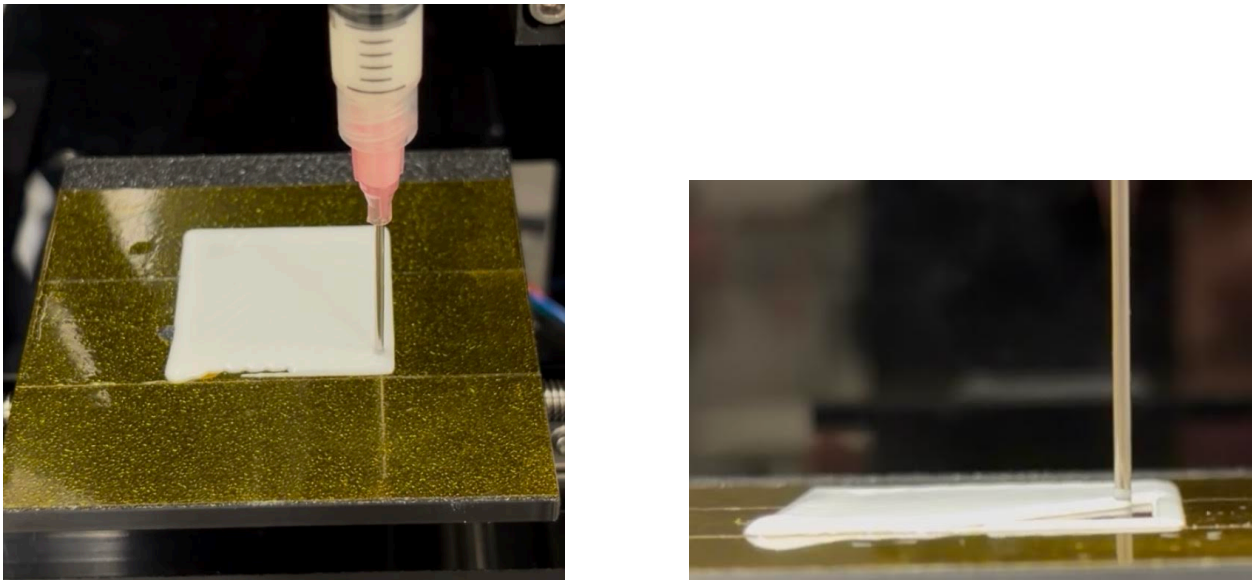

(a) Toothpaste print. **(b)** Close-up.

Figure 12: Toothpaste test print.

3.8 Platform Outcome

These results confirmed that the printer was mechanically stable, electronically functional, and capable of controlled deposition of high-viscosity materials. This provided a usable platform for the later lignin formulation and printing work.

Once I started working with the lignin formulations, it became clear that the higher-viscosity material placed much greater load on the syringe drive than the earlier surrogate tests. Extruding these mixtures required higher motor force, which in turn put more strain on the support structure around the plunger and syringe holder. Because of that, some hardware upgrades were needed to reduce flex and improve dimensional accuracy during extrusion. In Figure **??**a, the original support could bend backward when the motor pushed down on the plunger. That meant part of the motor motion was being lost into structural deflection instead of being transferred directly into extrusion. The upgraded support shown in Figure **??**b used a thicker and stiffer geometry, which reduced this bending and improved force transfer.

The syringe holder also needed improvement. In the earlier configuration shown in Figure 13c, only part of the syringe body was supported. Under load, this made it easier for the syringe to tilt or bend downward slightly during extrusion. The updated configuration in Figure 13d provided support over more of the syringe body, which reduced bending and helped make extrusion more consistent. These upgrades were useful because the high-viscosity lignin mixtures made small mechanical compliance issues much more obvious than they had been during initial toothpaste testing.

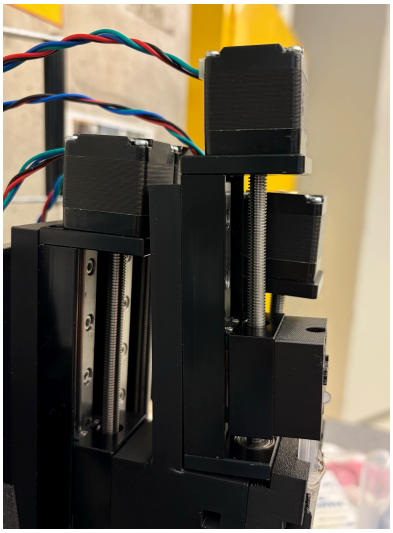

(a) Original support that bent under load.

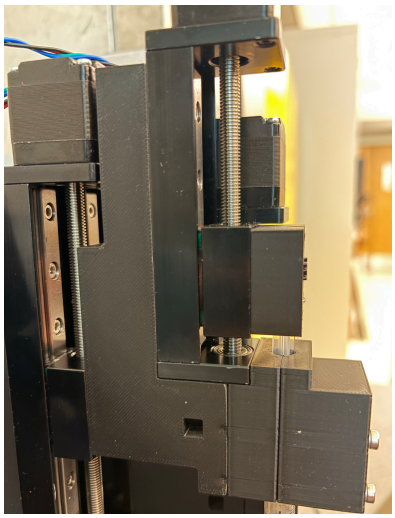

(b) Thickened, stiffer upgraded support.

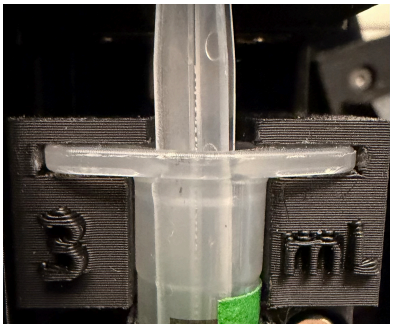

(c) Earlier syringe support with only partial backing.

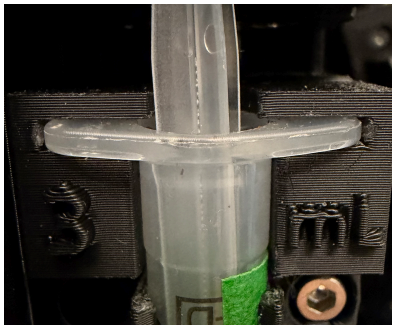

(d) Improved syringe support over more of the body.

Figure 13: Hardware upgrades introduced to improve stiffness and reduce deflection under high extrusion load.

Future improvements were also identified from this stage of the work. Better motor cooling would help during longer or higher-force prints, and further improvements to frame rigidity and bed leveling would help overall repeatability. Another promising direction is the use of conical nozzle tips, as shown in Figure 14. A conical tip gives a smoother flow transition into the nozzle and can reduce abrupt contraction losses. For viscous inks, that can lower the required extrusion pressure and improve flow stability at the nozzle entrance.

Figure 14: Example conical nozzle tip considered as a future improvement for reducing entry losses during extrusion.

4 Materials and Methods

4.1 Materials

The formulation work focused on a lignin–Pluronic F127 system. Two alkali lignins were explored: Sigma-Aldrich product 370959, with reported pH 6.5 in aqueous solution, and Sigma-Aldrich product 471003, with reported pH 10.5 [12, 13]. Based on the listed 100 g package prices accessed on April 22, 2026, these corresponded to approximately CAD \$1.63/g for 370959 and CAD \$0.94/g for 471003 [12, 13].

Pluronic F127 was selected because of its shear-thinning behaviour and widespread use in aqueous gel systems [1, 11]. The specific material used in this work was Sigma-Aldrich product P2443. Based on the listed 250 g package price of CAD \$82.50 accessed on April 22, 2026, this corresponds to approximately CAD \$33.00 per 100 g [17].

4.2 Formulation Approach

The lignin–F127 system was prepared in two stages. First, a water–F127 base mixture was made using 80 wt% water and 20 wt% Pluronic F127. This mixture was stirred and then kept under refrigerated conditions so that the F127 could dissolve fully at low temperature. This cold preparation step was important because F127 is thermoresponsive: at lower temperature it behaves more like a free-flowing liquid, while at higher temperature it becomes more viscous and tends toward gel formation [11]. In practice, that meant the water–F127 mixture was easier to prepare and handle when cold, but its consistency could change quickly after it was removed from the fridge and warmed during mixing or printing.

Once the water–F127 base was prepared, lignin was added to produce the final printable mixture. The lignin:(F127 + water) ratio was varied during screening. The literature reported that printable formulations could be prepared over a range from about 0.8:1 to 1.6:1 (lignin):(F127 + water), with a 1:1 ratio giving a strong balance of printability and strength in the reported system [1]. In this project, I used that range as a practical guide, then ad-

justed the ratio based on syringe extrudability and shape retention on the Printess platform.

After the basic mixing route was established, pH was introduced as a separate variable. Rather than adjusting the pH after the full ink had already been made, the pH of the water was changed before adding F127. The F127 was then dissolved into this pH-adjusted water, and lignin was added afterward. In practice, the addition of F127 did not appear to change the pH substantially, so the pH of the initial water phase remained a useful way to distinguish the different formulation routes tested.

4.3 Lignin Route Screening

I first compared the pH 6.5 and pH 10.5 alkali lignins. The pH 10.5 lignin was initially attractive because it was water-soluble, but it formed a putty-like material and showed visible water separation under pressure. The pH 6.5 lignin required more preparation, but it produced a more paste-like and workable mixture. That result pushed the project toward the lower-pH route.

(a) pH 10.5 lignin route.

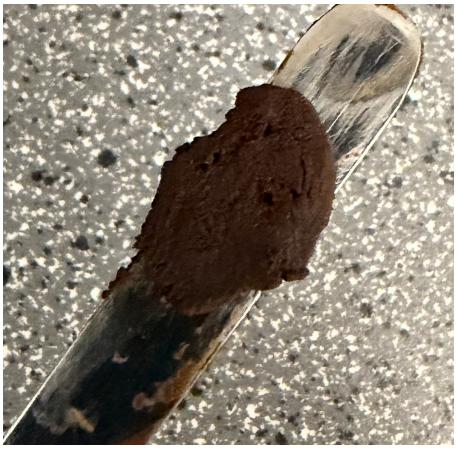

(b) pH 6.5 lignin route.

Figure 15: Visual comparison of the two alkali lignin routes examined during screening.

4.4 Lignin Preparation

Once I selected the pH 6.5 route, I used a preparation sequence to reduce agglomerates and improve consistency. The process consisted of:

1. tip sonication;
2. centrifugation;
3. drying through either air drying or freeze drying; and
4. dynamic light scattering (DLS) to compare the two drying routes.

Dynamic light scattering was then used to compare prepared lignin after air drying and freeze drying. The freeze-dried material showed a smaller apparent Z-average particle size than the air-dried material, while the air-dried material showed a lower PDI. The measured values are summarized in Table 3.

Table 3: Summary of DLS results for prepared lignin after two drying routes.

Drying route	Z-average (nm)	PDI
Freeze dried	1027	0.7408
Air dried	2217	0.4487

The DLS results suggested that freeze drying reduced the apparent average particle size. However, the freeze-dried sample was also more polydisperse, and both datasets carried quality warnings. In practice, the printing differences between the two drying routes were limited. Because of that, air drying remained attractive because it was much simpler.

4.5 Ink Preparation

Three different pH values were tested for the water–F127 phase: pH 5, pH 7, and pH 9. The pH 7 mixture was left neutral and contained only water and F127, while the pH 5 and pH 9 mixtures were adjusted using acidic and basic solutions, respectively. Changing the pH had a clear effect on the behaviour of the final lignin mixture. Lower-pH mixtures were thinner and allowed higher lignin loading, while higher-pH mixtures were thicker and crumblier. A 1:1.2 lignin:(F127 + water) ratio prepared with pH 5 water–F127 was selected as the most practical formulation.

Initially, the mixtures were compared using a simple practical screening test to judge whether their viscosity was suitable for printing. This was done by observing how easily each mixture could be pushed through an 18-gauge syringe and whether it could still hold its shape after extrusion. This gave a quick sense of which mixtures were too thick, too thin, or potentially suitable for use in the printer. Once the most promising formulations had been identified, formal viscosity testing was carried out. A major challenge during this stage was that the material became much thicker and more viscous as it warmed up and was exposed to air. Because of this, the mixtures had to be tested or printed almost immediately after mixing. The pH 9 sample thickened too quickly during testing, making the results less reliable than intended, although it was still clear that it was much thicker than the lower-pH mixtures. In practice, the machine could not even reach the same desired offset as easily because a much larger load was required.

Because of these issues, the pH 9 viscosity dataset was not treated as reliable for quantitative comparison. Instead, Figure 16 shows the pH 5 viscosity result together with a literature viscosity plot for a lignin/F127/water system from Jiang *et al.* [1]. The pH 5 formulation in this work showed the same general shear-thinning trend as the literature system, with viscosity decreasing strongly as shear rate increased. At the same time, the mixture used

in this work still appeared to be significantly thicker than the literature system across much of the plotted range. This suggests that the formulation, preparation history, or testing conditions were not directly equivalent, and more controlled rheology testing would be needed to properly understand the discrepancy. Since the material in this project changed quickly after mixing and air exposure, the present viscosity result should be treated as a useful practical indication rather than a fully reliable quantitative comparison.

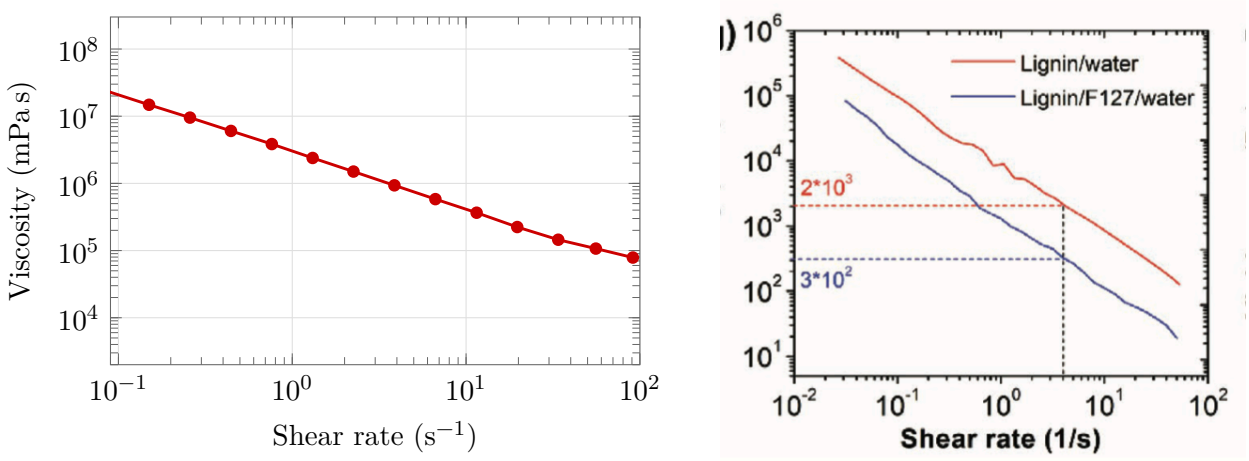

(a) Practical viscosity result for the pH 5 formulation used in this work.

(b) Literature viscosity comparison for lignin/F127/water, adapted from Jiang et al. [1].

Figure 16: Comparison between the pH 5 viscosity result measured in this work and the reported shear-thinning behaviour of a lignin/F127/water system in the literature.

4.6 Printing and Post-Processing

Printing was carried out using the completed Printess-based platform. The nozzle used in testing had a diameter of 0.965 mm. Printed samples were freeze-dried immediately after deposition and then thermally stabilized at 100 °C for two hours.

5 Results and Discussion

5.1 Printer Performance

The completed printer achieved stable axis motion, reliable syringe actuation, and a repeatable CAD-to-print workflow. The successful toothpaste test showed that the hardware could deposit a paste-like material before I introduced lignin inks.

The main platform limitations were stiffness, motor thermal management, and bed levelling. These effects were still visible during printing trials, especially in line-spacing tests. Because

the material and the machine were being developed at the same time, it was important to separate hardware-related issues from formulation-related issues as much as possible.

5.2 Printability and Post-Processing Behaviour

After the formulation screening described in Section 4, the pH 5 lignin–F127 mixture was used for the main printing trials. Line-spacing tests were used to assess practical printability. These tests showed that the printer could deposit repeated filaments with useful shape retention, but they also highlighted sensitivity to bed levelling and spacing consistency. Figure 17 shows representative trials printed with a 0.965 mm nozzle.

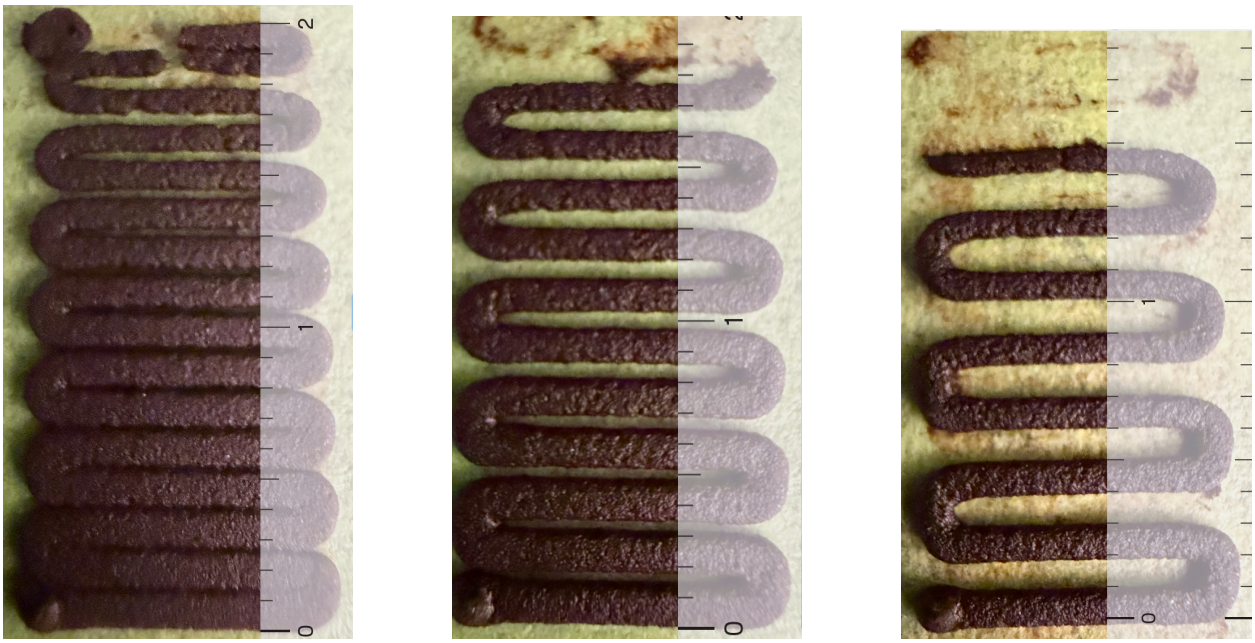

(a) 0.25 mm spacing. **(b)** 0.50 mm spacing. **(c)** 1.00 mm spacing.

Figure 17: Representative line-spacing tests printed through a 0.965 mm nozzle.

After freeze-drying, the samples felt much stiffer and showed noticeably better mechanical behaviour than comparable air-dried samples, which were brittle and crumbly. The most important post-processing result, however, was that thermal stabilization was essential. Samples were freeze-dried after printing and were fully water-soluble before heat treatment. After stabilization at 100 °C for two hours, they were no longer water-soluble, remained stable in oil, and became less prone to crumbling. This stability in oil is important because many potential applications may involve contact with oils, lubricants, or other non-aqueous environments, so the material must be able to maintain its structure under those conditions. Thermal stabilization also appeared to improve the overall strength of the samples. Before stabilization, the samples floated in water. After stabilization, they sank in both water and oil and stayed intact rather than dissolving. The overall process was:

$$\text{Print} \rightarrow \text{Freeze-dry} \rightarrow \text{Thermal stabilize at } 100\,^{\circ}\text{C for } 2\text{ h}$$

Figure 18: Printed ring structures immediately after printing, before freeze-drying and thermal stabilization.

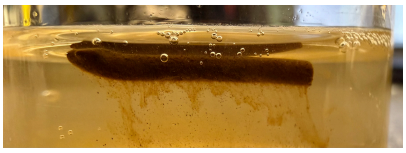

(a) Before thermal stabilization in water.

(b) After thermal stabilization in water.

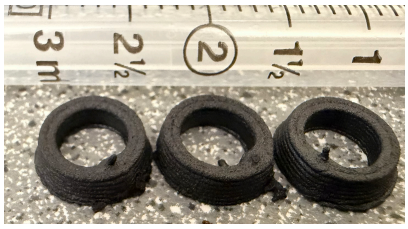

(c) Printed rings after freeze-drying and thermal stabilization.

Figure 19: Post-processing outcome of printed samples after freeze-drying and thermal stabilization.

5.3 Compression Testing

A simple compression assessment was carried out using printed rings with an outer diameter of approximately 10 mm and a wall thickness of about 2 mm. The specimens used for this test had already been freeze-dried and thermally stabilized. These samples were able to withstand about 15 lb of compressive load before failure. Taking 15 lb as approximately 66.7 N, and using an annular cross-sectional area based on a 10 mm outer diameter and 2 mm wall thickness, this corresponds to an approximate compressive stress of about 1.3 MPa. This is reasonably close to the compressive strength reported by Jiang *et al.*, who reported a value of 1.31 MPa for their lignin–F127 system [1].

Because this test was carried out using added weights rather than a standardized mechanical testing machine, it should only be treated as a rough preliminary estimate.

5.4 Material Behaviour and Limitations

The printed material showed clear mechanical limitations. It performed better under compression than under bending, where it was noticeably brittle and prone to fracture. This suggests that the weakness was not only due to poor interlayer bonding, but was also related to the inherent behaviour of the material itself.

Despite these limitations, the project still provided a useful foundation for future work. While the material was not fully optimized, the study helped identify the main factors influencing printability, handling, and post-processing performance. This is valuable because it gives a clearer direction for improving the formulation in later experiments.

6 Conclusion

I developed and validated a low-cost direct ink writing platform for lignin-based materials using the open-source Printess architecture. The completed system was assembled, wired, integrated with firmware, and operated using a repeatable CAD-to-print workflow. Surrogate toothpaste printing confirmed that the platform was capable of controlled deposition, and the total build cost was approximately CAD $585.

On the materials side, lignin–Pluronic F127 was identified as the most practical starting ink system for this platform. Of the two alkali lignins examined, the pH 6.5 lignin produced a more workable paste-like mixture than the pH 10.5 lignin. A final formulation of 1:1.2 lignin:(F127 + water) prepared with pH 5 water–F127 gave the best practical balance between extrusion and shape retention.

The printed structures showed useful initial shape retention, although print quality remained sensitive to bed levelling and formulation consistency. Post-processing was essential. After freeze-drying and thermal stabilization at 100 °C for two hours, the samples became water-stable and mechanically more robust. The processed material remained brittle in bending but performed better in compression.

Overall, this work showed that a low-cost open-source DIW system can be successfully built and used for preliminary lignin-based printing. It also showed that lignin preparation, formulation pH, and post-processing strongly influence the final printability and material behaviour. While the ink system is still at an early stage, it shows potential for applications where sustainable, high-lignin-content printed structures are desirable, particularly in low-load or non-structural geometries. This work provides a practical starting point for future refinement of both the printing platform and the material formulation.

References

[1] Bo Jiang, Yonggang Yao, Zhiqiang Liang, Jinlong Gao, Gegu Chen, Qinqin Xia, Ruiyu Mi, Miaolun Jiao, Xizheng Wang, and Liangbing Hu. Lignin-based direct ink printed structural scaffolds. *Small*, page 1907212, 2020. doi: 10.1002/smll.201907212.

[2] Maria Balk, Michael Schroeter, Eduardo da Conceicao, Nicole Schneider, Matthias Heuchel, Yvonne Pieper, Susanne Schwanz, Navid Khani, Hanin Alkhamis, Katarzyna Polak-Krasna, Axel T. Neffe, and Francesca M. Toma. Room-temperature, aqueous-based 3d printing of fully recyclable wood-like inks from upcycled lignin. *ACS Sustainable Chemistry & Engineering*, 2026. doi: 10.1021/acssuschemeng.5c07974.

[3] Lisa-Sophie Ebers and Marie-Pierre Laborie. Direct ink writing of fully bio-based liquid crystalline lignin/hydroxypropyl cellulose aqueous inks: Optimization of formulations and printing parameters. *ACS Applied Bio Materials*, 3:6897–6907, 2020. doi: 10.1021/acsabm.0c00804.

[4] Jonathan D. Weiss, Alana Mermin-Bunnell, Fredrik S. Solberg, Tony Tam, Luca Rosalia, Amit Sharir, Dominic Rutsche, Soham Sinha, Perry S. Choi, Masafumi Shibata, Yellappa Palagani, Riya Nilkant, Kiruthika Paulvannan, Michael Ma, and Mark A. Skylar-Scott. A low-cost, open-source 3d printer for multimaterial and high-throughput direct ink writing of soft and living materials. *Advanced Materials*, 37:2414971, 2025. doi: 10.1002/adma.202414971.

[5] Bo Jiang, Huan Jiao, Xinyu Guo, Gegu Chen, Jiaqi Guo, Wenjuan Wu, Yongcan Jin, Guozhong Cao, and Zhiqiang Liang. Lignin-based materials for additive manufacturing: Chemistry, processing, structures, properties, and applications. *Advanced Science*, 10: 2206055, 2023. doi: 10.1002/advs.202206055.

[6] Jian Yang, Xingye An, Bin Lu, Haibing Cao, Zhengbai Cheng, Xin Tong, Hongbin Liu, and Yonghao Ni. Lignin: A multi-faceted role/function in 3d printing inks. *International Journal of Biological Macromolecules*, 267:131364, 2024. doi: 10.1016/j.ijbiomac.2024.131364.

[7] Penghui Li, Jianpeng Ren, Zhengwei Jiang, Lijing Huang, Caiwen Wu, and Wenjuan Wu. Review on the preparation of fuels and chemicals based on lignin. *RSC Advances*, 12:10289–10305, 2022. doi: 10.1039/D2RA01341J.

[8] Mingming Yang, Hailong Li, Jing Shen, Shujun Li, Shouxin Liu, Jian Li, Zhijun Chen, Meng Li, and Tony D. James. Repurposing lignin to generate functional afterglow paper. *Cell Reports Physical Science*, 3(5):100867, 2022. doi: 10.1016/j.xcrp.2022.100867.

[9] Jingyu Liu and Cheng Yan. 3d printing of scaffolds for tissue engineering. In *Tissue Engineering Strategies for Organ Regeneration*. IntechOpen, 2018. doi: 10.5772/intechopen.78145.

[10] Maryam Borghei, Hossein Baniasadi, Roozbeh Abidnejad, Rubina Ajdary, Seyedabolfazl Mousavihashemi, Daria Robertson, Jukka Niskanen, Eero Kontturi, Tanja Kallio, and Orlando J. Rojas. Wood flour and kraft lignin enable air-drying of the nanocellulose-based 3d-printed structures. *Additive Manufacturing*, 92:104397, 2024. doi: 10.1016/j.addma.2024.104397.

[11] Irving K. Schmolka. Artificial skin i. preparation and properties of pluronic f-127 gels for treatment of burns. *Journal of Biomedical Materials Research*, 6:571–582, 1972.

[12] Sigma-Aldrich. Lignin, alkali, product 370959. https://www.sigmaaldrich.com/CA/en/product/aldrich/370959, 2026. Accessed April 22, 2026.

[13] Sigma-Aldrich. Lignin, alkali, product 471003. https://www.sigmaaldrich.com/CA/en/product/aldrich/471003, 2026. Accessed April 22, 2026.

[14] Printess Project. Printess low-cost 3d printer. https://github.com/weiss-jonathan/Printess-Low-Cost-3D-Printer, 2025. Accessed April 21, 2026.

[15] Marlin Firmware. Marlin firmware documentation. https://marlinfw.org/, 2026. Accessed April 21, 2026.

[16] UltiMaker. Ultimaker cura. https://ultimaker.com/software/ultimaker-cura, 2026. Accessed April 21, 2026.

[17] Sigma-Aldrich. Pluronic f-127, product p2443. https://www.sigmaaldrich.com/CA/en/product/sigma/p2443, 2026. Accessed April 22, 2026.